JACS
JOURNAL OF THE AMERICAN CHEMICAL SOCIETY
Article
Cite This: J. Am. Chem. Soc. 2019, 141, 11286−11297
pubs.acs.org/JACS

Delayed Photoluminescence in Metal-Conjugated Fluorophores

Mingrui Yang,[†,∥] Pavel Moroz,[†,‡] Zhicheng Jin,[§] Darya S. Budkina,[†,∥] Nida Sundrani,[‡] Dmitry Porotnikov,[†,∥] James Cassidy,[†,∥] Yuya Sugiyama,[⊥] Alexander N. Tarnovsky,[†,∥] Hedi Mattoussi,[§] and Mikhail Zamkov*[,†,‡]

[†]The Center for Photochemical Sciences, [‡]Department of Physics, and [∥]Department of Chemistry, Bowling Green State University, Bowling Green, Ohio 43403, United States

[§]Department of Chemistry, Biochemistry, Florida State University, Tallahassee, Florida 32303, United States

[⊥]Asahi-Kasei Corporation, Healthcare R&D Center, 2-1 Samejima, Fuji City, Shizuoka 416-8501 Japan

Supporting Information

ABSTRACT: Assemblies of metal nanostructures and fluorescent molecules represent a promising platform for the development of biosensing and near-field imaging applications. Typically, the interaction of molecular fluorophores with surface plasmons in metals results in either quenching or enhancement of the dye excitation energy. Here, we demonstrate that fluorescent molecules can also engage in a reversible energy transfer (ET) with proximal metal surfaces, during which quenching of the dye emission via the energy transfer to localized surface plasmons can trigger delayed ET from metal back to the fluorescent molecule. The resulting two-step process leads to the sustained delayed photoluminescence (PL) in metal-conjugated fluorophores, as was demonstrated here through the observation of increased PL lifetime in assemblies of Au nanoparticles and organic dyes (Alexa 488, Cy3.5, and Cy5). The observed enhancement of the PL lifetime in metal-conjugated fluorophores was corroborated by theoretical calculations based on the reverse ET model, suggesting that these processes could be ubiquitous in many other dye−metal assemblies.

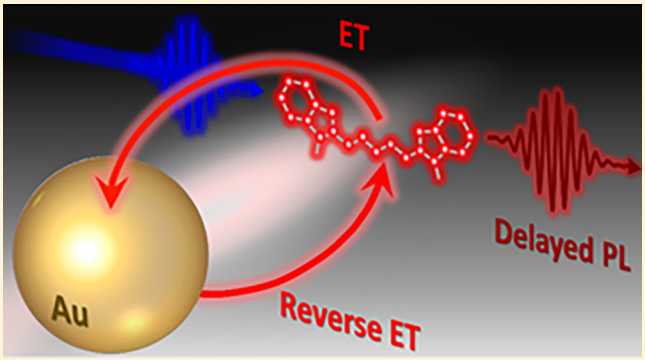

INTRODUCTION

The interaction of fluorescent dyes with proximal metal surfaces can result in either the enhancement[1−5] or quenching[6−15] of the dye photoluminescence (PL). The ultimate change in the PL intensity is determined by the specific nature of electric dipole−dipole interactions at the molecule−metal interface that can shift the energy transfer (ET) balance in either direction. For instance, PL quenching[16−21] is commonly observed when the surface plasmon band of a metal nanoparticle has a significant spectral overlap with the emission profile of a dye, favoring the transfer of its excitation energy via Förster or nanosurface energy transfer mechanisms. Such metal-induced quenching of the dye PL has recently evolved into a popular strategy of signal transduction in biosensing[22−31] and near-field imaging applications.[22,32−34] The realization of the metal-enhanced fluorescence,[35−44] on the other hand, demands more stringent requirements to be met by a dye−metal system, which include the spectral overlap in the excitation region, spatial alignment of dye and metal electric dipoles, and the absence of the photoinduced charge transfer between the two components. Under these conditions, the excitation energy in a metal could be transferred to a proximal dye through the plasmon-induced resonant energy transfer (PIRET),[4,45−49] also known as the field enhancement mechanism.[40,50−52] Examples of the PIRET process in dye−metal assemblies have been witnessed in photocatalytic,[49,52−60] photovoltaic,[61−67] and biosensing[22−24,27,35,68,69] applications of metal nanoparticles.

From a theoretical standpoint, the interaction of fluorescent molecules with surface plasmons in metals is usually treated as an incoherent process,[70] which excludes the possibility of the reversible energy transfer between the two components. Consequently, quenching of the dye PL is usually not considered to result in the enhancement of the excitation energy in the metal. This scenario, however, is not characteristic of localized surface plasmons in metal nanoparticles, where the energy accepted from a proximal dye could be resonantly transferred back to conjugated molecules due to the absence of Stokes shifts associated with nonradiative emission by metals[45,71] (no vibrational relaxation losses). Furthermore, an electric dipole of a metal nanoparticle excited via the dye → metal ET would be aligned with a dipole of the energy-donating molecule, such that the rate of the corresponding reverse metal → dye energy transfer process could exceed that of the polarization-averaged field enhancement in the same

Received: May 7, 2019
Published: June 23, 2019

DOI: 10.1021/jacs.9b04697
J. Am. Chem. Soc. 2019, 141, 11286−11297

dye−metal system. In order to account for a coherent excitation transfer in a metal−fluorophore assembly, the interaction of fluorescent molecules with metal surfaces must be treated as reversible, which assumes that the loss of dye excitations ($-dN_{dye}$) augments the population of metal plasmons ($+dN_{metal}$) and vice versa. This scenario is possible when the system is excited in the vicinity of the exciton−plasmon resonance ($h\omega_{pl} \approx h\omega_{exciton}$), a condition met by many dye−metal assemblies.[4,21,72,73]

Here, we report on the experimental observation of the reversible energy transfer in assemblies of Au nanoparticles and fluorescent molecules (Alexa 488, Cy3.5, Cy5). The present study reveals that quenching of the dye emission via FRET or NSET to localized surface plasmons in Au nanoparticles is followed by the backward transfer of metal excitations to dye molecules (Figure 1). Such a delayed repopulation of the dye

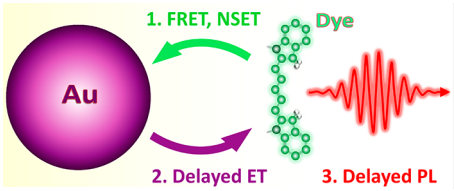

Figure 1. Illustration of the forward (dye → AuNP) and reverse (AuNP → dye) energy transfer. Quenching of the dye PL via Förster resonant energy transfer (FRET) or nanosurface energy transfer (NSET) results in the excitation of localized surface plasmons in Au NPs. The induced excitation energy in the metal can subsequently be transferred back to surface-anchored dyes (via the PIRET mechanism). The resulting two-step energy transfer process, therefore, can cause the repopulation of the dye excitation energy, which is evidenced as the delayed photoluminescence in conjugated dyes.

excitation energy was manifested in this work through the observation of an increased PL lifetime of Au-conjugated dyes in comparison to nonconjugated molecules. Ultrafast transient absorption measurements have confirmed the delayed rise of the excitation energy in Au-conjugated fluorophores, which was temporally correlated with the excited-state decay in polymer-capped Au nanoparticles. Notably, relative amplitudes of the reverse metal → dye ET in each of the three investigated samples were found proportional to the respective metal-induced PL enhancement factors, determined using polarization-averaged sample transmitted excitation photoluminescence (STEP) spectroscopy. Theoretical calculations based on the reversible ET model were subsequently employed to explain the observed PL lifetime enhancement in dye−AuNP assemblies, suggesting that such processes could be ubiquitous in many other dye−metal systems. Considering the significant role that metal−dye assemblies play in many areas of science and technology, the present findings could have important implications for the development of biological sensors, light-emitting materials, and light-harvesting assemblies.[22,24,26,35,74−82]

RESULTS AND DISCUSSION

Early studies of the metal-enhanced fluorescence[83−92] have identified the existence of several competing processes that contribute to the energy exchange between a metal nanoparticle and a semiconducting fluorophore. In the absence of charge-transfer interactions, quenching of the fluorophore emission is usually described by the dye to metal FRET,[93] NSET,[94] or the Gersten−Nitzan[95] mechanisms (nonradiative quenching), whereas the PL enhancement process is attributed to the metal → dye PIRET (field enhancement).[45,46,70] When the two processes are incoherent (absence of the back and forth transfer), their cumulative effect on emission changes in metal-coupled fluorophores (ΔFL) can be expressed using a weak-coupling[96] dipole−dipole approximation, as follows:[49]

$$\begin{aligned}\Delta FL &= \frac{FL_{dye-metal}}{FL_{dye}} \\ &= \Delta FL_{PIRET} \times \Delta FL_{ET} \\ &= (1 + E_{PIRET}) \times (1 - E_{ET}) \\ &= \left(1 + \frac{\alpha_{plasmon}}{\alpha_{dye}} \times \frac{1}{1 + (R/R_0^{PIRET})^n}\right) \\ &\quad \times \left(1 - \frac{1}{1 + (R/R_0^{ET})^n}\right)\end{aligned} \quad (1)$$

where n = 4−6 depending on whether the dipoles are considered to be surface- or pointlike, α represents the wavelength-dependent absorption coefficient, and R^{ET}_0 is the donor−acceptor distance corresponding to the 50% efficiency for nonradiative dye energy quenching (via FRET or NSET).

The competition of metal-induced FL quenching (ΔFL < 1) and field enhancement (ΔFL > 1) processes is well documented in the literature. Typically, quenching prevails when the size of a metal nanoparticle falls below 20 nm.[6−9,97] In this size regime, quenching via FRET or NSET, as well as the photoinduced charge transfer back to metal, overwhelm the effect of PIRET-based enhancement.[20,97] Meanwhile, the plasmon-enhanced fluorescence (ΔFL > 1) is usually observed in systems featuring large-diameter metal nanoparticles (>30 nm in size)[4,83,88,91,98−103] and metal nanorods,[104−108] where slower dephasing surface plasmons exhibit a greater probability of interacting with semiconductor excitons through the PIRET mechanism. In the case of weakly emitting dyes, the PL gain may be further increased by the plasmon enhancement of the semiconductor radiative rates,[8,109,110,94] although a radiative rate reduction has also been predicted for chemically conjugated dyes.[9]

In the present study, the interaction of fluorescent molecules with localized surface plasmons was investigated by using three dye−metal assemblies comprising 14.4 nm Au nanoparticles (a characteristic TEM image is shown in Figure SF5) conjugated with Alexa 488, Cy3.5, and Cy5 dye molecules. Au NP surfaces were capped with a lipoic acid (LA)-containing polymer[111] with an average thickness of 4−6 nm. The three types of fluorophores were chosen to represent different regimes of the spectral overlap between the molecular absorption range and the surface plasmon band, as shown in Figure 2. The Cy3.5−AuNP assembly exhibited the strongest overlap in the absorption range, which was expected to enhance the corresponding "reverse" AuNP → Cy3.5 energy transfer rate. Meanwhile, the absorption bands of Alexa 488 and Cy5 dyes were offset toward the higher and lower energy regions of the Au NP absorption maximum, respectively. In terms of PL quenching, the Alexa 488 assembly exhibited the strongest emission−absorption overlap, favoring the Alexa → AuNP ET, while PL emission spectral ranges for Cy3.5 and Cy5 were red-shifted from the Au absorption maximum. The conjugation protocol was performed according to a previous report,[111] as

DOI: 10.1021/jacs.9b04697
J. Am. Chem. Soc. 2019, 141, 11286−11297

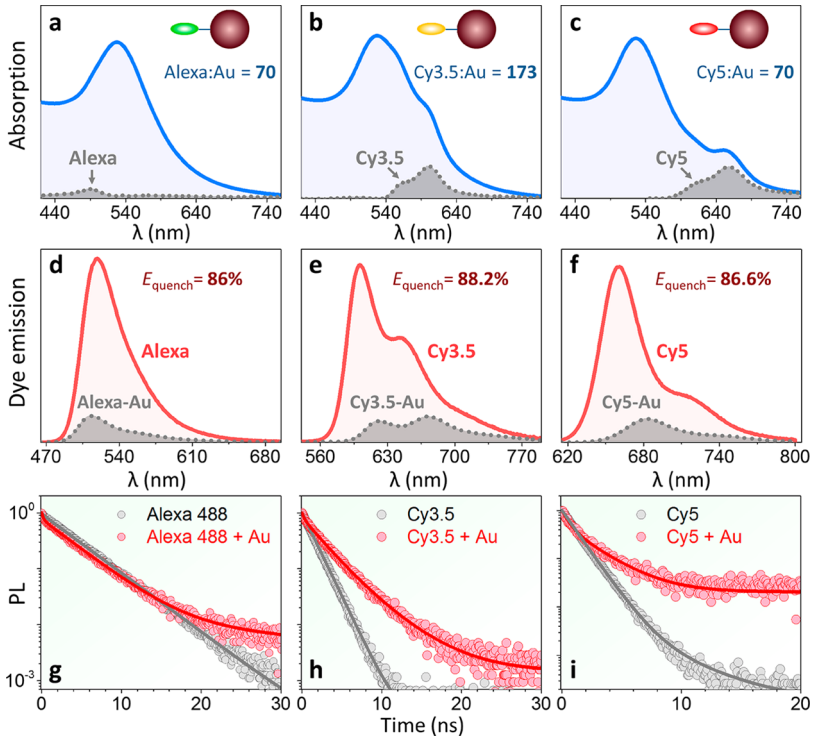

Figure 2. (a–c) Absorption profiles of three dye–AuNP assemblies comprising 14.4 nm Au nanoparticles conjugated to (a) Alexa 488, (b) Cy3.5, and (c) Cy5 dye molecules. The inserts show approximate dye to AuNP molar ratios estimated from known extinction coefficients. (d–f) Emission profiles of the three dye molecules before (dark red) and after (gray) conjugation to Au nanoparticles. The PL intensity quenching ratios for each case are shown. (g–i) PL lifetimes of the three investigated dye molecules before (gray) and after (red) conjugation to Au nanoparticles. Notably, the PL lifetimes of Cy3.5–AuNP in (h) and Cy5–AuNP in (i) are increased relative to those of isolated molecules.

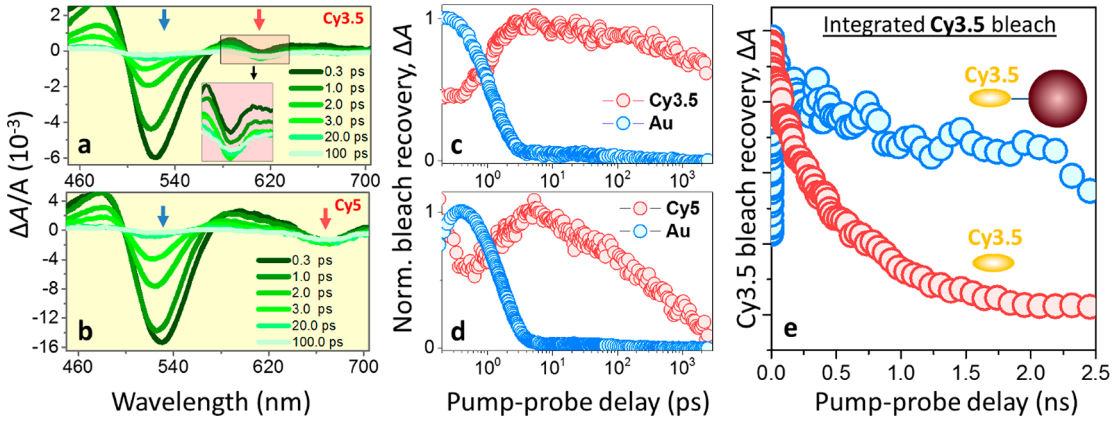

Figure 3. Summary of ultrafast transient absorption (TA) measurements. (a) Transient absorption spectra of Cy3.5–AuNP assemblies. TA bleach features corresponding to AuNP and Cy3.5 dye components are indicated by blue and red arrows, respectively. The pump excitation wavelength was set to λ_{exc} = 590 nm. (b). Transient absorption spectra of Cy5–AuNP assemblies, where blue and red arrows indicate the TA bleach in AuNP and Cy5 dye, respectively. The pump excitation wavelength was set to λ_{exc} = 640 nm. (c). Integrated TA bleach recovery corresponding to Cy3.5 (red) and AuNP (blue) spectral ranges of a Cy3.5–AuNP system, shown in (a). The rise of the Cy3.5 bleach amplitude at short pump–probe delays (τ < 3 ps) is attributed to the 3 ps recovery of the spectrally broad photoinduced absorption in Au nanoparticles. (d) Integrated TA bleach recovery corresponding to Cy5 (red) and AuNP (blue) spectral ranges of the Cy5–AuNP system, shown in (b). (e). Comparison of the Cy3.5 bleach recovery before (red) and after (blue) conjugation with Au nanoparticles. The increased lifetime of the excited-state population in Au-conjugated dyes is consistent with the observation of increased PL intensity decay in Cy3.5–AuNP assemblies.

illustrated in the diagram of Figure SF1. The dye–AuNP product was characterized using ^{1}H NMR (Figure SF2), dynamic light scattering (Figure SF3), and exclusion column filtration (Figure SF4).

The conjugation of fluorescent dyes with Au nanoparticles has resulted in 7–8-fold quenching of the steady-state emission for all three investigated samples, as illustrated in Figure 2d–f. Considering the substantial spectral overlap between the surface plasmon band and emission profiles of Alexa 488 (Figure 2d), Cy3.5 (Figure 2e), and Cy5 (Figure 2f), the reduction in the PL intensity in all cases was attributed primarily to dye → AuNP nonradiative quenching via resonant energy transfer (FRET, NSET). The photoinduced charge transfer from the excited dye to a metal surface was considered

DOI: 10.1021/jacs.9b04697
J. Am. Chem. Soc. 2019, 141, 11286–11297

as another possible mechanism of PL quenching,[112] which affected the subpopulation of conjugated molecules exhibiting electrical coupling with Au.

Contrary to expectations based on dye → AuNP energy transfer scenario, the changes in the PL lifetime of Au-conjugated dyes (Figure 2g–i) were not proportional to their respective PL quenching efficiencies. The difference was particularly prominent in the case of Cy3.5–AuNP assemblies, where, despite an 88.2% reduction in the Cy3.5 PL intensity (ΔI = 0.12), the corresponding lifetime was increased almost 2-fold relative to that of isolated fluorophores, $\Delta\tau \approx 2$ (Figure 2h). A similar trend was observed for Cy5–AuNP assemblies, where the PL lifetime was increased upon conjugation (Figure 2i), despite a 7-fold reduction in the total emission intensity (Figure 2f). The Alexa 488–AuNP assembly was the only system that showed a slight PL lifetime reduction upon conjugation (Figure 2g). Nevertheless, the relative change in the PL lifetime of Au-anchored Alexa 488 ($\Delta\tau \approx 1$) did not correspond to the change in the emission intensity (ΔI = 0.14).

The increase in the excited-state lifetime of metal-conjugated Cy3.5 and Cy5 fluorophores was corroborated by ultrafast transient absorption (TA) measurements (Figure 3 and Figure SF6). To determine the lifetime of dye excitations in dye–AuNP and dye-only samples, chirp-corrected TA spectra were recorded in the 0.3–2.5 ns time interval (see Figure 3a,b). Excitation at the high-energy side of the dye absorption range (λ_{exc} = 590 nm for Cy3.5–AuNP and λ_{exc} = 640 nm for Cy5–AuNP) has caused an instantaneous bleach of both the dye and metal nanoparticle excitation transitions, as indicated in Figure 3a,b by red and blue arrows, respectively. The negative ΔA feature in the TA spectra of Au nanoparticles (blue arrow) is known to arise from excitation-induced broadening of the surface plasmon peak, which causes a characteristic spectral "dip" at the plasmon wavelength sandwiched by the two positive "wings".[113,114] Such broadening of the plasmon absorbance results from nondipolar plasma oscillations in Au nanoparticles induced by the excitation pulse.

According to the time-dependent evolution of the spectrally integrated Cy3.5 TA bleach in Figure 3e, the recovery of excitations in dye-only Cy3.5 samples (red curve) was substantially faster than the corresponding bleach recovery in Cy3.5–AuNP assemblies (blue curve). The difference in the excited state decay time between dye–metal and dye-only samples was very similar to the difference observed in measurements of the PL intensity decay. Indeed, over the 2.5 ns pump–probe delay range, depicted in Figure 3e, the recovery of Au-conjugated Cy3.5 appears to be at least twice as slow as in isolated Cy3.5 molecules. This observation provides strong evidence that excited-state lifetimes of Cy3.5 dyes increase upon conjugation with Au NPs.

In addition to a slower decay of excited states in metal-conjugated dyes, the TA dynamics of Cy3.5–AuNP and Cy5–AuNP assemblies showed some other interesting features. At early pump–probe times (τ < 3 ps), metal-conjugated dyes exhibited a fast rise of the excited-state population, which was not observed in isolated molecules (Figure 3c,d). In this case, no correlation between the early onset of the dye bleach and the decay of plasmon excitations in Au NPs was inferred. In particular, a careful analysis of TA traces was able to attribute the initial growth of the spectrally integrated bleach in Cy3.5 and Cy5 dyes (Figure 3c,d, red curve) to the early-time background contribution. According to Figure 3a,b and Figure SF6, TA spectra of Au-conjugated dyes contained a spectrally broad, positive feature associated with the photoinduced absorption (PA) in metals (positive "wings"),[115] which effectively reduced the amplitude of the dye bleach in dye–metal assemblies. On the basis of these observations, we conclude that the early-time recovery of the TA bleach in Au domains (Figure 4a, blue circles) did not correlate with the rise of the TA bleach in Cy3.5 dyes (Figure 3a, red circles). This refers to both hot electron and resonant energy transfer

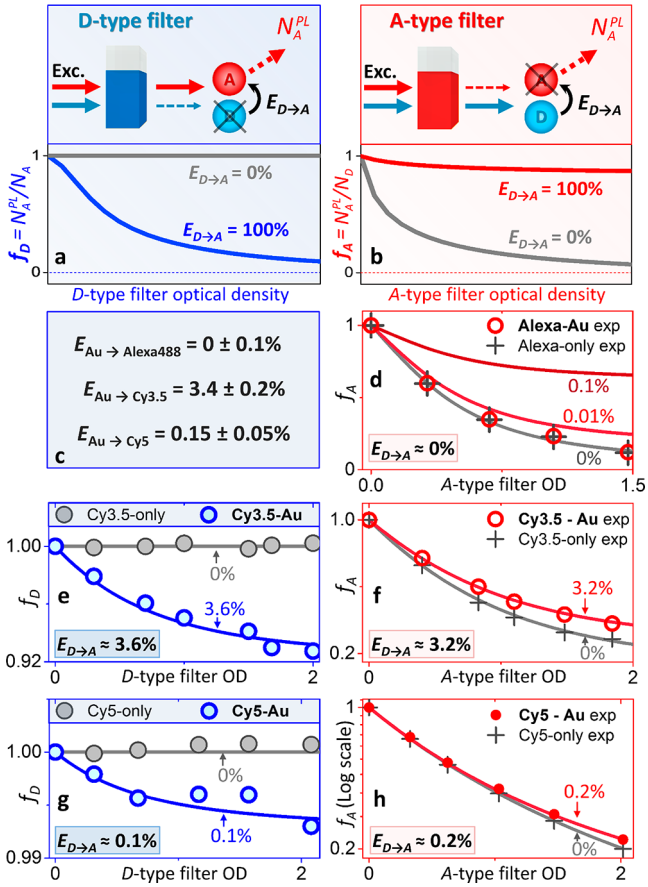

Figure 4. Illustration of the STEP technique for measurements of the Au → dye energy transfer efficiency, which relies on either (a) Au-donor type or (b) dye-acceptor type excitation filters. The broad-band excitation light is passed through a respective excitation filter (Au-donor type, solutions of CdSe/CdS nanocrystals, which spectrally match the plasmon absorption of Au NPs; dye-acceptor type, Alexa 488, Cy3.5, Cy5), which causes the acceptor emission, N_A^{PL}, to change proportionally to the energy transfer efficiency, $E_{D\to A}$. To obtain the $E_{D\to A}$ value, the measured f ratio (f_A or f_D, see text) is fitted with a model parametric curve, $f_{theor}(E_{D\to A})$, featuring a single fitting parameter, $E_{D\to A}$. (c) Summary of STEP measurements for all three investigated dye–Au assemblies. (d) STEP measurements of $E_{D\to A}$ in Alexa 488–AuNP assemblies utilizing an acceptor-type filter. The observed set of experimental f_A is consistent with $E_{D\to A} \approx 0\%$. (e) STEP measurements of $E_{D\to A}$ in Cy3.5–AuNP assemblies utilizing a donor-type filter. The observed experimental f_D values are best fitted with a model curve utilizing $E_{D\to A}$ = 3.6%. (f) STEP measurements of $E_{D\to A}$ in Cy3.5–AuNP assemblies utilizing an acceptor-type filter. The observed experimental f_A values are best fitted with a model curve utilizing $E_{D\to A}$ = 3.2%. (g) Donor-type STEP measurements of $E_{D\to A}$ in Cy5–AuNP assemblies resulting in $E_{D\to A}$ = 0.1%. (h) Acceptor-type STEP measurements of $E_{D\to A}$ in Cy5–AuNP assemblies resulting in $E_{D\to A}$ = 0.2%.

DOI: 10.1021/jacs.9b04697
J. Am. Chem. Soc. 2019, 141, 11286–11297

processes, as the former mechanism does not enhance the Cy3.5 TA bleach signal beyond the aforementioned PA effect, while the AuNP → Cy3.5 PIRET process is generally too fast (<50 fs) to be resolved in present TA measurements (pump pulse duration ∼120 fs).

The presence of a long-lived PL component in the decay of Cy3.5 and Cy5 dyes (and to a lesser extent in Alexa 488) suggests the existence of the excited-state repopulation process ($dN_{dye}(t) > 0$). As was stated above, the AuNP → dye PIRET resulting from the direct excitation of Au nanoparticles and the hot electron transfer have relatively short decay times to contribute to such a long-lived excited state of metal-conjugated fluorophores (>1 ns). In this regard, any possible mechanism that could result in a continuous repopulation of metal-conjugated dyes must involve an excited-state reservoir, which slowly feeds the excitation energy to a dye. Under these considerations, one possible mechanism of the delayed PL in metal-conjugated dyes could be attributed to a two-step excitation transfer process, involving the dye → metal energy transfer followed by the metal → dye PIRET. This scenario is schematically illustrated in Figure 1. The reverse PIRET process is triggered by the ET from a dye molecule and, therefore, is temporally delayed relative to the initial excitation event. The Au to dye energy transfer could be mediated by an LA-containing polymer shell, which accepts the initial excitation energy from a metal. The evidence in favor of such metal → polymer excitation transfer is seen in the TA spectra of Au−polymer composites (Figure SF10) as a spectrally broad photoinduced absorption. The long-lived positive ΔA feature implies that new states in a Au−polymer assembly become occupied as the plasmon excitation relaxes. The decay of these states can therefore induce a delayed excitation of conjugated dyes. Considering that surface plasmons induced by the energy transfer from conjugated dyes are dipole-aligned with the electric field of the donating molecule, the reverse plasmon → dye energy transfer could be more efficient than a "direct" PIRET process.

In order to understand whether the proposed "reverse" energy transfer via the field enhancement is feasible in investigated dye−metal systems, we have performed sample transmitted excitation photoluminescence (STEP) measurements of the metal-enhanced PL in all three samples. STEP spectroscopy[116−119] was recently introduced for measurements of the ET efficiency, $E_{D\to A}$, in systems with nonemissive donor species (e.g., plasmonic nanoparticles). It is based on the assumption that the number of photons emitted by an acceptor fluorophore, N_A^{PL}, depends linearly on the number of excited acceptor (A) and donor (D) molecules, N_A and N_D, respectively:

$$N_A^{PL} = QY_A(N_A + E_{D\to A}N_D) \quad (2)$$

where QY_A is the emission quantum yield of the fluorophore A in the presence of the donor D (as measured in the donor−acceptor assembly). The $E_{D\to A}$ parameter represents the percentage of donor excitations that are transferred non-radiatively to the acceptor moiety. To determine $E_{D\to A}$, the donor−acceptor sample is excited using a broad-band light source and the emission intensity of the acceptor dye $N_A^{PL}(E)$ is recorded. The excitation light is then spectrally shaped using donor-like or acceptor-like filters (Figure 4a,b) designed to suppress the excitation of Au NP donor or dye acceptor species in the investigated sample ($N_D \ll N_A$ or $N_A \ll N_D$, respectively). If the spectral profile of the excitation light, $n(\lambda)$, and the optical density (OD) of the excitation filter are known, one can predict the change in the acceptor emission as a function of a single parameter, $E_{D\to A}$ (see Figure SF9). It should be noted that eq 2 does account for the loss of the acceptor (dye quenching) excitations due to the dye → Au ET. This is because quenching of the dye emission lowers the effective QY_A in eq 2. The corresponding reduction, ΔQY_A, is the same with and without the excitation filter present since Au nanoparticles do not need to be excited to accept energy from a proximal dye. As a result, the value of QY_A cancels out from the equation for $E_{D\to A}$, as shown in the diagram of Figure SF9.

Figure 4ab illustrates the procedure for extracting the energy transfer efficiencies from STEP measurements utilizing the two types of excitation filters. A donor-type excitation filter is used to suppress the excitation of donor molecules in the sample, causing the acceptor emission to change proportionally to $E_{D\to A}$ (Figure 4a). These changes are best illustrated by plotting a normalized dye-acceptor emission, $f_D = N_A^{PL}/N_A$, as a function of the donor-type filter optical density, as shown for the two limiting cases of $E_{D\to A}$: E = 100% and E = 0%. Conversely, an acceptor-like excitation filter (e.g., a solution of acceptor dye molecules) can be used to selectively suppress the excitation of acceptor molecules, such that the energy transfer efficiency, $E_{D\to A}$, could be obtained from the acceptor emission scaled by the number of donor excitations, $f_D = N_A^{PL}/N_D$, as illustrated in Figure 4b. To reduce an experimental error, present STEP measurements were performed through sequential injections of the reference (dye-only) and dye−AuNP samples into the target cuvette without realigning the optical setup or changing the filter solution (see Methods in the Supporting Information for details). Such a reference-based measurement strategy has allowed for the experimental uncertainty to be contained within 1−2%.

Figure 4 summarizes the results of STEP measurements. Out of three investigated dye−AuNP systems, the Cy3.5−AuNP assembly resulted in the highest value of the PIRET efficiency. According to the analysis in Figure 4e, the f_D ratio corresponding to Cy3.5-only samples was essentially independent of the Au-donor type filter OD, as was expected in this case due to the lack of donor (Au) contribution into the dye emission. Conversely, for Cy3.5−AuNP samples, the experimental f_D ratio (blue circles) decreased with the filter OD, indicating the contribution of Au excitations to the Cy3.5 emission. The measured f_D was fitted with a model parametric curve, f_{theor}, featuring a single fitting parameter, $E_{D\to A}$, where $f_{theor}(E) = N_A^{PL}(E)/N_A$, was determined using eq 2 as a parametric function of the energy transfer efficiency, E. As shown in Figure 5e, the average PIRET efficiency for Cy3.5−AuNP samples was determined to be 3.6%. This value represents the percentage of Au-absorbed excitations that were transferred to the entire population of proximal Cy3.5 dyes. In other words, the group of surface-anchored dyes was treated as a single acceptor moiety. STEP measurements of the same sample, utilizing an acceptor-like excitation filter (Figure 4f), have yielded a slightly lower value for $E_{D\to A}$, which equaled 3.2%. Consequently, we conclude that the average metal → dye ET efficiency for a Cy3.5−AuNP system was 3.4%, which represents the PIRET efficiency averaged over different molecular orientations ($\kappa^2 \approx 2/3$). In the case of Cy5−AuNP samples, the PIRET efficiency was found to be 0.15% (Figure 4g,h). A relatively lower value of $E_{D\to A}$ for Cy5−AuNP assemblies (in comparison to Cy3.5−AuNP) was consistent

DOI: 10.1021/jacs.9b04697
J. Am. Chem. Soc. 2019, 141, 11286−11297

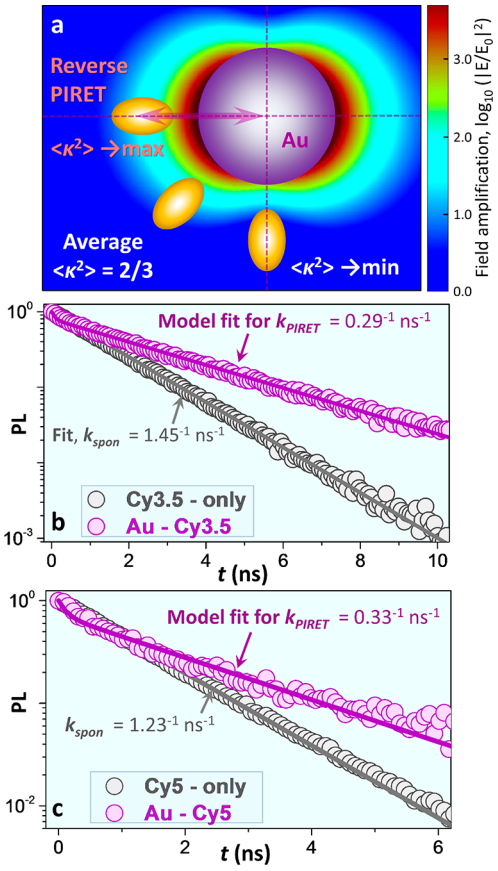

Figure 5. (a) Comparison of surface plasmon electric field amplitudes for aligned and isotopically oriented dye molecules. The reverse PIRET is expected to result in a preferential alignment of metal and dye dipoles ($\kappa^2 \approx 4$). The electric field intensity amplification was calculated for a spherical Au nanoparticle ($\varepsilon = -8.4953 + 1.6239i$) using the T matrix linking of outgoing (Hankel) and incident (Bessel) fields, as detailed in refs 117 and 122. (b) Fitting the delayed PL in Cy3.5−AuNP assemblies (purple circles) with the solution of coupled rate equations (eqs 3 and 4) on the basis of the reverse ET model (purple curve). The best fit is obtained for $k_{PIRET} = (0.29\ ns)^{-1}$. The emission of nonconjugated Cy3.5 is shown by gray circles. (c) Fitting the delayed PL in Cy5−AuNP assemblies (purple circles) with the solution of coupled rate equations on the basis of the reverse ET model (purple curve). The best fit was obtained for $k_{PIRET} = (0.33\ ns)^{-1}$. The emission of nonconjugated Cy5 is shown by gray circles.

with a reduced spectral overlap, F, between Au and Cy5 species in the excitation spectral range ($F_{Cy3.5}/F_{Cy5} \approx 2.7$). In the case of Alexa 488−AuNP samples, Au-donor-type STEP measurements could not be performed due to a significant spectral cross talk between the surface plasmon band and acceptor (Alexa 488) emission profile. Consequently, on the basis of only dye-acceptor type measurements, we determined that the metal to dye PIRET in this case was close to zero, $E_{D\to A} \approx 0.0 \pm 0.1$ (Figure 4d). It should be noted, however, that due to a relatively high ratio of optical extinction coefficients in Au and Alexa 488 dye (~1400), the transfer of up to 0.1% of the excitation energy from a Au nanoparticle to about 70 surface-appended dyes is sufficient to increase the Alexa 488 emission by 3−4% ($\Delta FL \leq 1.03-1.04$, see section 2e in the Supporting Information).

STEP measurements of the polarization-averaged ET efficiencies in Figure 4 suggest that "instantaneous" plasmon → dye energy transfer can occur in all three systems with the highest rate expected in Cy3.5−AuNP assemblies and the lowest in Alexa 488−AuNP. By taking into account the relative nanoparticle/dye extinction ratios and the average number of conjugated dyes, we estimate that, for a single direct excitation absorbed by one of the Cy3.5 dyes on the surface of Au, it receives an average of 0.31 excitations from the metal nanoparticle (please see section 2e in the Supporting Information for details of calculations). For instance, if PL quenching due to FRET or NSET were negligible, the resulting PL enhancement due to proximal Au would have been 31% ($\Delta FL = 1.31$). For Cy5 and Alexa 488, the estimated increase in the exciton population due to the plasmon-induced energy transfer from Au was ~6% ($\Delta FL = 1.06$) and ~3.5% ($\Delta FL \leq 1.035$), respectively. Notably, the latter value represents the upper bound rather than the average efficiency due to large experimental uncertainties.

The experiment manifestation of the metal to dye energy transfer in Cy3.5−AuNP and Cy5−AuNP assemblies supports our hypothesis that the reverse PIRET process is possible in these systems. As was previously mentioned, the reverse PIRET rate is expected to be enhanced relative to polarization-averaged ET observed in STEP measurements due to the favorable orientation of the surface plasmon and exciton electric dipoles. This concept is illustrated in Figure 5a, which compares the amplitude of the plasmon electric field (d_{Au} = 14.4 nm) for aligned and isotopically oriented molecules. Since quenching of the dye emission gives rise to surface plasmons that are dipole-aligned with the fluorophore electric field, the orientation factor κ^2 for these molecules is assumed to be maximized ($\kappa^2 \approx 4$). In comparison to the isotropic orientation of dipoles observed in STEP measurements ($\kappa^2 \approx 2/3$), the corresponding enhancement of the Förster radius for the reverse PIRET $R_0^{aligned}/R_0^{isotropic}$ is expected to range between 1.35 and 1.56, depending on whether metal dipoles are considered to be point- or surfacelike.

To model the coherent energy exchange in Cy3.5−AuNP and Cy5−AuNP assemblies, which includes the possibility of a reverse PIRET, we assume that the number of excitations in Au-conjugated dye molecules (N_{dye}) can grow proportionally to the number of surface plasmon excitations in Au (N_{metal}) caused by the reverse PIRET mechanism. Under this assumption, the temporal evolution of N_{dye} and N_{metal} populations can be determined by solving coupled rate equations that include the metal → dye energy transfer rate (k_{PIRET}):

$$dN_{dye}/dt = -k_{spon}N_{dye} - k_{ET}N_{dye} + k_{PIRET}N_{metal} \quad (3)$$

$$dN_{metal}/dt = -k_{PIRET}N_{metal} - k_{metal*}N_{metal} + k_{ET}N_{dye} \quad (4)$$

where k_{ET} is the PL quenching rate due to the dye to metal FRET and NSET, k_{spon} is the rate of a spontaneous decay in nonconjugated dyes, and k_{metal*} is the rate of the excitation decay in metal. We assume that any modifications of k_{spon} due to the stimulated-emission effect of metal surfaces are negligible in systems with strong emitters. Indeed, since the interaction of surface plasmons with proximal dyes is short-lived (<50 fs), a significant change in the value of k_{spon} is expected only if the nonradiative decay rate greatly exceeds the rate of radiative processes (weakly emitting fluorophores). This is not the case for strongly emitting Cy3.5 and Cy5 fluorophores exhibiting PL quantum yields over 30%.[120,121]

The value of k_{metal*} is nominally determined by the rate of the plasmon energy relaxation in Au NPs. Due to the presence

DOI: 10.1021/jacs.9b04697
J. Am. Chem. Soc. 2019, 141, 11286−11297

of a surrounding polymer matrix, however, the excitation energy in metal could be thermalized into long-lived states of a polymer or a polymer−dye interface. This could be attested by the long-lived photoinduced absorption feature observed in TA measurements of LA-PIMA-PEG-capped Au NPs (positive ΔA in Figure SF10). The relaxation of this PA feature (∼100 ps) is more than 10^3 times slower than the plasmon dephasing time constant. We therefore propose that the presence of the polymer matrix effectively extends the lifetime of plasmon excitations in Au NPs.

The results of model calculations for the PL decay in Cy3.5−AuNP and Cy5−AuNP assemblies are summarized in Figure 5b,c, as well as in Table 1. Out of four independent parameters entering eqs 3 and 4, k_{spon}, k_{ET}, k_{PIRET}, and k_{metal*}, the first two were acquired from experimental measurements. The value of k_{spon} was obtained from the single-exponential fit of the PL intensity decay for nonconjugated dyes (gray curve in Figure 5b,c), while the initial value of k_{ET} was determined by assuming that nonradiative energy transfer was the sole process responsible for PL quenching in Au-conjugated dyes. In the case of Cy3.5−AuNP assemblies, this yielded: $k_{ET} = k_{spon} \times E_Q/(1 - E_Q) = (0.21\ ns)^{-1}$, where $E_Q = 0.882$ is the PL quenching efficiency. In order to include any non-ET contributions to PL quenching (e.g., dye → Au photoinduced charge transfer), the above equation was modified to $k_{ET} + k_{non\text{-}ET} = k_{spon} \times E_Q/(1 - E_Q)$, which effectively reduced the value of the k_{ET} parameter. To allow for small adjustments of the ET rate during the fitting procedure, both k_{ET} and k_{PIRET} parameters were allowed to be varied in a self-consistent manner in order to obtain the best fit of the experimental PL intensity decay. In the case of Cy3.5−AuNP assemblies, the ultimate value of $k_{ET} = (0.32\ ns)^{-1}$, resulting from a model fit, was 34% lower than the initial $k_{ET} = (0.21\ ns)^{-1}$, suggesting that 34% of excitations in Cy3.5 are likely to be depleted by non-ET processes (e.g., dye → Au charge transfer). The resulting PIRET rate, $k_{PIRET} = (0.29\ ns)^{-1}$, was found to be similar to the k_{ET} value, indicating that the excitation energy transfer to and from the dye molecule occurred with comparable rates. The similarity of k_{ET} and k_{PIRET} parameters could be explained by the nearly symmetric overlap integrals associated with ET (e.g., FRET, NSET) and PIRET processes (see eq 1).

Table 1. Summary of Model Calculations for the Three Conjugated Systems, Showing k^{-1}_{spon}, k^{-1}_{ET}, and k^{-1}_{PIRET} Inverse Rates[a]

	Alexa 488−AuNP	Cy3.5−AuNP	Cy5−AuNP
k^{-1}_{spon} (ns)	4.06	1.45	1.23
k^{-1}_{ET} (ns)	1.9	0.32	0.51
k^{-1}_{PIRET} (ns)	0.15	0.29	0.33

[a]The first parameter was determined by fitting the PL intensity decay of nonconjugated dyes, while the last two rates were obtained by solving coupled rate equations (eqs 3 and 4).

The results of model calculations for the Cy5−AuNP system are shown in Figure 5c and Table 1. The value of $k_{spon} = (1.23\ ns)^{-1}$ was determined by fitting the PL intensity decay in nonconjugated Cy5 samples (gray curve), while the initial value of $k_{ET} = k_{spon}E_Q/(1 - E_Q) = (0.19ns)^{-1}$ was estimated from the quenching efficiency. Coupled rate equations were then solved in a self-consistent manner to obtain the best fit of the experimental PL decay for the Cy5−AuNP system (Figure 5c, purple curve). The resulting ET rate, $k_{ET} = (0.51\ ns)^{-1}$, was found to be lower than its initial assessment of $(0.19\ ns)^{-1}$ determined from $E_Q = 0.866$. Accordingly, we estimate that PL quenching in Cy5−AuNP assemblies could be contributed up to 63% by non-ET processes. Such a non-ET contribution to Cy5 PL quenching could arise from Au-conjugated molecules that share the electron density with the metal surface (e.g., molecules that are in direct electrical contact with Au) and therefore essentially dark. Due to their absorption contribution, these dyes are accounted for in calculations of PL *intensity* quenching (ΔI), but not in the PL *lifetime* measurements ($\Delta\tau$). Finally, the PL lifetime enhancement effect in model calculations based on eqs 3 and 4 could be reproduced only by assuming that k_{metal*} was much lower than k_{spon}. This condition was necessary for the excited state "reservoir" that feeds the dye excitation population to exist. The exact nature of such an excited state, however, could not be determined in this work.

In the case of Alexa 488−AuNP colloids, the application of the fitting procedure based on eqs 3 and 4 was only partially successful (see Figure SF7). While the model reproduced the long-term decay component accurately, the early-time PL decay could not be fit well using a reasonable range of k_{ET} and k_{PIRET} parameters. The discrepancy between the experimental and simulated PL intensities for $t < 1$ ns could be attributed to the contribution of short-lived processes that were not accounted for by the three rates in eqs 3 and 4. For instance, the dye → Au NP photoinduced charge transfer affecting a subpopulation of dyes that are electrically coupled to a metal surface represents one example of such processes. In regard to a long-term decay of the Alexa 488−AuNP emission, the fitting procedure has yielded a comparatively large value of k_{PIRET} (see Table 1) that exceeded the corresponding rates in Cy3.5−AuNP and Cy5−AuNP samples.

One of the key questions raised by the present investigation concerns the lack of previous reports of the reverse PIRET process in dye−metal assemblies. According to the majority of publications reporting PL intensity decay measurements, the conjugation of dyes with metal nanoparticles results in the reduction of the PL lifetime.[9,16,44,97,123−130] Only one other study[131] has reported a 1.5-fold enhancement in the PL lifetime of Au-conjugated Cy3 fluorophores despite ∼41% PL intensity quenching. After a careful examination of the existing literature, we were not able to determine any particular condition that was responsible for a different trend observed in the PL lifetime by both the present work and ref 131, as similar dye−metal assemblies (e.g., Cy5-DNA−AuNP) were also reported to result in the reduced PL lifetime by other groups.[125] Nevertheless, the present observation of the enhanced PL lifetime was supported by transient absorption measurements, clearly showing that the excited-state population in Au-conjugated dyes exhibits a longer lifetime than in isolated molecules. Such PL lifetime enhancement in metal-coupled fluorophores can be predicted for an arbitrary dye−metal assembly using the aforementioned coherent ET model (eqs 3 and 4) as a parametric function of k_{PIRET} and k_{ET} rates. As shown in Figure 6, the increase in the dye → metal ET rate relative to k_{spon} leads to a reduction in the PL lifetime of a conjugated fluorophore, $\Delta\tau = \tau_{dye-metal}/\tau_{dye} < 1$ (blue-green color region), which is commonly observed in PL quenching measurements. Meanwhile, when both k_{ET} and k_{PIRET} parameters are large (k_{ET}, $k_{PIRET} > k_{spon}$), an enhancement in

DOI: 10.1021/jacs.9b04697
J. Am. Chem. Soc. 2019, 141, 11286−11297

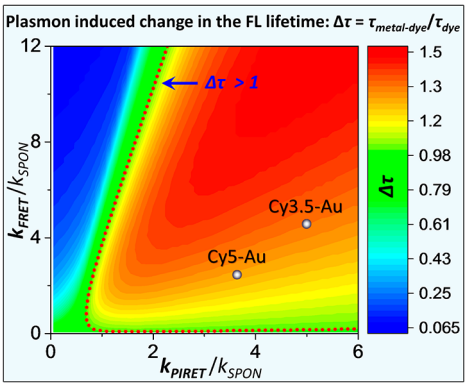

Figure 6. $\Delta\tau$ contour plot showing possible changes in the PL lifetime of a metal-conjugated dye ($\Delta\tau = \tau_{dye-metal}/\tau_{dye}$) as a function of k_{ET} and k_{PIRET} rates, respectively. Both nonradiative quenching ET and PIRET transfer rates are normalized by the dye's spontaneous decay rate (k_{spon}). The dotted red contour line encircles the parametric region where the PL lifetime of a conjugated dye is enhanced, $\Delta\tau > 1$, relative to its PL intrinsic lifetime.

the PL lifetime of a conjugated fluorophore $\Delta\tau > 1$ (orange-red color region) is expected.

CONCLUSIONS

Quenching of the dye fluorescence by proximal metal surfaces represent a popular strategy of determining intermolecular distances in biosensing and near-field imaging applications. The vast majority of experimental measurements rely on the reduction in the PL intensity of metal-conjugated fluorophores, ΔI, assuming that corresponding changes in the PL lifetime, $\Delta\tau$, are proportional. Our work demonstrates that this is not the case when the metal to dye energy transfer is significant. Under these conditions, the energy transferred from the photoexcited fluorophore to a metal nanoparticle could be transferred back to the conjugated molecule, causing an enhancement in the PL lifetime. The difference between ΔI and $\Delta\tau$ is expected to be particularly large when both the nonradiative quenching and PIRET rates are greater than the rate of the spontaneous decay. Consequently, metal–dye assemblies featuring a strong plasmon–exciton coupling are likely to exhibit different values of ΔI and $\Delta\tau$.

From a theoretical standpoint, the present observation of the enhanced PL lifetime in metal-conjugated dyes reveals the underlying coherent interaction between metal and molecular electric dipoles. By using a combination of time-resolved spectroscopy and rate-equation calculations, we showed that fluorescent molecules can engage in a reversible energy transfer with proximal metal surfaces, during which quenching of the dye emission via the energy transfer to localized surface plasmons triggers the delayed ET from the metal back to the fluorescent molecule. The reverse ET was shown to occur concurrently with PL quenching, which causes the PL lifetime of metal-conjugated fluorophores to increase despite an overall reduction of the dye emission intensity. The amplitude of the reversible ET in dye–metal assemblies was found to be proportional to the metal to dye energy transfer efficiency, determined by means of polarization-averaged STEP spectroscopy measurements. Theoretical simulations based on the coherent ET model were employed to explain the observed PL lifetime enhancement in Alexa 488–AuNP, Cy3.5–AuNP, and Cy5–AuNP assemblies, indicating that such processes could be pervasive in other dye–metal systems. Considering a broad scientific interest in metal-conjugated dye assemblies, the present findings could have an important scientific and technological impact on the development of biological sensors, light-emitting materials, and light-harvesting assemblies.

ASSOCIATED CONTENT

Supporting Information

The Supporting Information is available free of charge on the ACS Publications website at DOI: 10.1021/jacs.9b04697.

Experimental section, additional figures, and details of the calculations (PDF)

AUTHOR INFORMATION

Corresponding Author

*E-mail for M.Z.: zamkovm@bgsu.edu

ORCID

Hedi Mattoussi: 0000-0002-6511-9323

Mikhail Zamkov: 0000-0002-8638-2972

Notes

The authors declare no competing financial interest.

ACKNOWLEDGMENTS

This work was supported by Award DE-SC0016872 (M.Z.) funded by the U.S. Department of Energy, Office of Science. J.C. was partially supported by NSF Award DMR-1710063. H.M. acknowledges Asahi-Kasei, Inc., for financial support. TEM work was performed by Dr. Yan Xin at the National High Magnetic Field Laboratory, which is supported by National Science Foundation Cooperative Agreement No. DMR-1644779 and the State of Florida.

REFERENCES

(1) Tam, F.; Goodrich, G. P.; Johnson, B. R.; Halas, N. J. Plasmonic Enhancement of Molecular Fluorescence. *Nano Lett.* **2007**, *7*, 496–501.

(2) Chen, Y.; Munechika, K.; Ginger, D. S. Dependence of Fluorescence Intensity on the Spectral Overlap between Fluorophores and Plasmon Resonant Single Silver Nanoparticles. *Nano Lett.* **2007**, *7*, 690–696.

(3) Ayala-Orozco, C.; Liu, J. G.; Knight, M. W.; Wang, Y.; Day, J. K.; Nordlander, P.; Halas, N. J. Fluorescence Enhancement of Molecules Inside a Gold Nanomatryoshka. *Nano Lett.* **2014**, *14*, 2926–2933.

(4) Wang, M.; Rajeeva, B. B.; Scarabelli, L.; Perillo, E. P.; Dunn, A. K.; Liz-Marzán, L. M.; Zheng, Y. Molecular-Fluorescence Enhancement via Blue-Shifted Plasmon-Induced Resonance Energy Transfer. *J. Phys. Chem. C* **2016**, *120*, 14820.

(5) Thomas, K. G. Making Gold Nanoparticles Glow: Enhanced Emission from a Surface-Bound Fluoroprobe. *J. Am. Chem. Soc.* **2000**, *122*, 2655–2656.

(6) Jennings, T. L.; Singh, M. P.; Strouse, G. F. Fluorescent Lifetime Quenching Near d = 1.5 nm Gold Nanoparticles: Probing NSET Validity. *J. Am. Chem. Soc.* **2006**, *128*, 5462.

(7) Seelig, J.; Leslie, K.; Renn, A.; Kühn, S.; Jacobsen, V.; van de Corput, M.; Wyman, C.; Sandoghdar, V. Nanoparticle-induced Fluorescence Lifetime Modification as Nanoscopic Ruler: Demonstration at the Single Molecule Level. *Nano Lett.* **2007**, *7*, 685–689.

(8) Acuna, G. P.; Bucher, M.; Stein, I. H.; Steinhauer, C.; Kuzyk, A.; Holzmeister, P.; Schreiber, R.; Moroz, A.; Stefani, F. D.; Liedl, T.; Simmel, F. C.; Tinnefeld, P. Distance Dependence of Single-Fluorophore Quenching by Gold Nanoparticles Studied on DNA Origami. *ACS Nano* **2012**, *6*, 3189–3195.

(9) Dulkeith, E.; Morteani, A. C.; Niedereichholz, T.; Klar, T. A.; Feldmann, J.; Levi, S. A.; van Veggel, F.; Reinhoudt, D. N.; Möller,

M.; Gittins, D. I. Fluorescence Quenching of Dye Molecules near Gold Nanoparticles: Radiative and Nonradiative Effects. *Phys. Rev. Lett.* **2002**, *89*, 203002.
(10) Yun, C. S.; Javier, A.; Jennings, T.; Fisher, M.; Hira, S.; Peterson, S.; Hopkins, B.; Reich, N. O.; Strouse, G. F. Nanometal Surface Energy Transfer in Optical Rulers, Breaking the FRET Barrier. *J. Am. Chem. Soc.* **2005**, *127*, 3115−3119.
(11) Dulkeith, E.; Ringler, M.; Klar, T. A.; Feldmann, J.; Muñoz Javier, A.; Parak, W. J. Gold Nanoparticles Quench Fluorescence by Phase Induced Radiative Rate Suppression. *Nano Lett.* **2005**, *5*, 585−589.
(12) You, C. C.; Miranda, O. R.; Gider, B.; Ghosh, P. S.; Kim, I. B.; Erdogan, B.; Krovi, S. A.; Bunz, U. H. F.; Rotello, V. M. Detection and Identification of Proteins Using Nanoparticle-Fluorescent Polymer 'Chemical Nose' Sensors. *Nat. Nanotechnol.* **2007**, *2*, 318.
(13) Huang, C.-C.; Chang, H.-T. Selective Gold-Nanoparticle-Based "Turn-On" Fluorescent Sensors for Detection of Mercury(II) in Aqueous Solution. *Anal. Chem.* **2006**, *78*, 8332.
(14) Seferos, D. S.; Giljohann, D. A.; Hill, H. D.; Prigodich, A. E.; Mirkin, C. A. Nano-Flares: Probes for Transfection and mRNA Detection in Living Cells. *J. Am. Chem. Soc.* **2007**, *129*, 15477.
(15) Merkl, J. P.; Schmidtke, C.; Aldeek, F.; Safi, M.; Feld, A.; Kloust, H.; Mattoussi, H.; Lange, H.; Weller, H. Functional-Group-Dependent Formation of Bioactive Fluorescent-Plasmonic Nanohybrids. *J. Phys. Chem. C* **2016**, *120*, 25732−25741.
(16) Pons, T.; Medintz, I. L.; Sapsford, K. E.; Higashiya, S.; Grimes, A. F.; English, D. S.; Mattoussi, H. On the Quenching of Semiconductor Quantum Dot Photoluminescence by Proximal Gold Nanoparticles. *Nano Lett.* **2007**, *7*, 3157−3164.
(17) Fan, C.; Wang, S.; Hong, J. W.; Bazan, G. C.; Plaxco, K. W.; Heeger, A. J. Beyond Superquenching: Hyper-Efficient Energy Transfer from Conjugated Polymers to Gold Nanoparticles. *Proc. Natl. Acad. Sci. U. S. A.* **2003**, *100*, 6297−6301.
(18) Liu, D.; Wang, S.; Swierczewska, M.; Huang, X.; Bhirde, A. A.; Sun, J.; Wang, Z.; Yang, M.; Jiang, X.; Chen, X. Gold Nanoparticle Based Activatable Probe for Sensing Ultra-Low Levels of Prostate Specific Antigen. *ACS Nano* **2012**, *6*, 10999−11008.
(19) Chowdhury, S.; Wu, Z.; Jaquins-Gerstl, A.; Liu, S.; Dembska, A.; Armitage, B. A.; Jin, R.; Peteanu, L. A. Wavelength Dependence of the Fluorescence Quenching Efficiency of Nearby Dyes by Gold Nanoclusters and Nanoparticles: The Roles of Spectral Overlap and Particle Size. *J. Phys. Chem. C* **2011**, *115*, 20105−20112.
(20) Reineck, P.; Gómez, D.; Ng, S. H.; Karg, M.; Bell, T.; Mulvaney, P.; Bach, U. Distance and Wavelength Dependent Quenching of Molecular Fluorescence by Au@SiO_2 Core-Shell Nanoparticles. *ACS Nano* **2013**, *7*, 6636−6648.
(21) Aldeek, F.; Ji, X.; Mattoussi, H. Quenching of Quantum Dot Emission by Fluorescent Gold Clusters: What It Does and Does Not Share with the Förster Formalism. *J. Phys. Chem. C* **2013**, *117*, 15429−15437.
(22) Saha, K.; Agasti, S. S.; Kim, C.; Li, X.; Rotello, V. M. Gold Nanoparticles in Chemical and Biological Sensing. *Chem. Rev.* **2012**, *112*, 2739−2779.
(23) Demchenko, A. P. *Introduction to fluorescence sensing*; Springer: Amsterdam, 2009.
(24) Kumar, A.; Kim, S.; Nam, J. M. Plasmonically Engineered Nanoprobes for Biomedical Applications. *J. Am. Chem. Soc.* **2016**, *138*, 14509−14525.
(25) Dubertret, B.; Calame, M.; Libchaber, A. J. Single-Mismatch Detection Using Gold-Quenched Fluorescent Oligonucleotides. *Nat. Biotechnol.* **2001**, *19*, 365−370.
(26) Peltomaa, R.; Amaro-Torres, F.; Carrasco, S.; Orellana, G.; Benito-Peña, E.; Moreno-Bondi, M. C. Homogeneous Quenching Immunoassay for Fumonisin B1 Based on Gold Nanoparticles and an Epitope-Mimicking Yellow Fluorescent Protein. *ACS Nano* **2018**, *12*, 11333−11342.
(27) Samanta, A.; Medintz, I. L. Nanoparticles and DNA a Powerful and Growing Functional Combination in Bionanotechnology. *Nanoscale* **2016**, *8*, 9037−9095.
(28) Huang, T.; Murray, R. W. Quenching of $[Ru(bpy)_3]^{2+}$ Fluorescence by Binding to Au Nanoparticles. *Langmuir* **2002**, *18*, 7077−7081.
(29) Maxwell, D. J.; Taylor, J. R.; Nie, S. M. Self-Assembled Nanoparticle Probes for Recognition and Detection of Biomolecules. *J. Am. Chem. Soc.* **2002**, *124*, 9606−9612.
(30) Vietz, C.; Lalkens, B.; Acuna, G. P.; Tinnefeld, P. Synergistic Combination of Unquenching and Plasmonic Fluorescence Enhancement in Fluorogenic Nucleic Acid Hybridization Probes. *Nano Lett.* **2017**, *17*, 6496−6500.
(31) Tyrakowski, C. M.; Snee, P. T. Ratiometric CdSe/ZnS Quantum Dot Protein Sensor. *Anal. Chem.* **2014**, *86*, 2380−2386.
(32) Miyawaki, A.; Llopis, J.; Helm, R.; McCaffery, J. M.; Adams, J. A.; Ikura, M.; Tsien, R. Y. Fluorescent Indicators for Ca^{2+} Based on Green Fluorescent Proteins and Calmodulin. *Nature* **1997**, *388*, 882−887.
(33) Medintz, I. L.; Clapp, A. R.; Mattoussi, H.; Goldman, E. R.; Fisher, B.; Mauro, J. M. Self-Assembled Nanoscale Biosensors Based on Quantum Dot FRET Donors. *Nat. Mater.* **2003**, *2*, 630−638.
(34) Willard, D. M.; Mutschler, T.; Yu, M.; Jung, J.; Van Orden, A. Directing Energy Flow Through Quantum Dots: Towards Nanoscale Sensing. *Anal. Bioanal. Chem.* **2006**, *384*, 564−571.
(35) Aslan, K.; Gryczynski, I.; Malicka, J.; Matveeva, E.; Lakowicz, J. R.; Geddes, C. D. Metal-Enhanced Fluorescence: An Emerging Tool in Biotechnology. *Curr. Opin. Biotechnol.* **2005**, *16*, 55−62.
(36) Fu, B.; Flynn, J. D.; Isaacoff, B. P.; Rowland, D. J.; Biteen, J. S. Super-Resolving the Distance-Dependent Plasmon-Enhanced Fluorescence of Single Dye and Fluorescent Protein Molecules. *J. Phys. Chem. C* **2015**, *119*, 19350−19358.
(37) Ipe, B. I.; Yoosaf, K.; Thomas, K. G. Functionalized Gold Nanoparticles as Phosphorescent Nanomaterials and Sensors. *J. Am. Chem. Soc.* **2006**, *128*, 1907.
(38) Lisunova, M.; Mahmoud, M.; Holland, N.; Combs, Z. A.; El-Sayed, M. A.; Tsukruk, V. V. The Unusual Fluorescence Intensity Enhancement of Poly(P-Phenyleneethenylene) Polymer Separated From the Silver Nanocube Surface by H-bonded LbL Shells. *J. Mater. Chem.* **2012**, *22*, 16745−16753.
(39) Bardhan, R.; Grady, N. K.; Halas, N. J. Nanoscale Control of Near-Infrared Fluorescence Enhancement Using Au Nanoshells. *Small* **2008**, *4*, 1716−1722.
(40) Lee, J.; Govorov, A. O.; Dulka, J.; Kotov, N. A. Bioconjugates of CdTe Nanowires and Au Nanoparticles: Plasmon-Exciton Interactions, Luminescence Enhancement, and Collective Effects. *Nano Lett.* **2004**, *4*, 2323−2330.
(41) Erdem, T.; Soran-Erdem, Z.; Hernandez-Martinez, P. L.; Sharma, V. K.; Akcali, H.; Akcali, I.; Gaponik, N.; Eychmüller, A.; Demir, H. V. Sweet Plasmonics: Sucrose Macrocrystals of Metal Nanoparticles. *Nano Res.* **2015**, *8*, 860−869.
(42) Mackowski, S.; Wörmke, S.; Maier, A. J.; Brotosudarmo, T. H. P.; Harutyunyan, H.; Hartschuh, A.; Govorov, A. O.; Scheer, H.; Bräuchle, C. Metal-Enhanced Fluorescence of Chlorophylls in Single Light-Harvesting Complexes. *Nano Lett.* **2008**, *8*, 558−564.
(43) Razgoniaeva, N.; Lambright, S.; Sharma, N.; Acharya, A.; Khon, E.; Moroz, P.; Razgoniaev, A.; Ostrowski, A. D.; Zamkov, M. Exciton Generation in Semiconductor Nanocrystals via the Near-Field Plasmon Energy Transfer. *J. Phys. Chem. C* **2015**, *119*, 15562.
(44) Munechika, K.; Chen, Y.; Tillack, A. F.; Kulkarni, A. P.; Jen-La Plante, I.; Munro, A. M.; Ginger, D. S. Spectral Control of Plasmonic Emission Enhancement from Quantum Dots near Single Silver Nanoprisms. *Nano Lett.* **2010**, *10*, 2598−2603.
(45) Li, J.; Cushing, S. K.; Meng, F.; Senty, T. R.; Bristow, A. D.; Wu, N. Plasmon-Induced Resonance Energy Transfer for Solar Energy Conversion. *Nat. Photonics* **2015**, *9*, 601−607.
(46) Wu, N. Plasmonic Metal−Semiconductor Photocatalysts and Photoelectrochemical Cells: A Review. *Nanoscale* **2018**, *10*, 2679−2696.
(47) Thimsen, E.; Le Formal, F.; Gratzel, M.; Warren, S. C. Influence of Plasmonic Au Nanoparticles on the Photoactivity of Fe_2O_3 Electrodes for Water Splitting. *Nano Lett.* **2011**, *11*, 35−43.

DOI: 10.1021/jacs.9b04697
J. Am. Chem. Soc. 2019, 141, 11286−11297

(48) Cushing, S. K.; Li, J.; Meng, F.; Senty, T. R.; Suri, S.; Zhi, M.; Li, M.; Bristow, A. D.; Wu, N. Photocatalytic Activity Enhanced by Plasmonic Resonant Energy Transfer from Metal to Semiconductor. *J. Am. Chem. Soc.* **2012**, *134*, 15033−15041.
(49) Kholmicheva, N.; Royo Romero, L.; Cassidy, J.; Zamkov, M. Prospects and Applications of Plasmon-Exciton Interactions in the Near-Field Regime. *Nanophotonics* **2019**, *8*, 613−628.
(50) Shimizu, K. T.; Woo, W. K.; Fisher, B. R.; Eisler, H. J.; Bawendi, M. G. Surface-Enhanced Emission from Single Semiconductor Nanocrystals. *Phys. Rev. Lett.* **2002**, *89*, 117401.
(51) Jiang, J.; Bosnick, K.; Maillard, M.; Brus, L. Single Molecule Raman Spectroscopy at the Junctions of Large Ag Nanocrystals. *J. Phys. Chem. B* **2003**, *107*, 9964.
(52) Liu, Z.; Hou, W.; Pavaskar, P.; Aykol, M.; Cronin, S. B. Plasmon Resonant Enhancement of Photocatalytic Water Splitting Under Visible Illumination. *Nano Lett.* **2011**, *11*, 1111−1116.
(53) Warren, S. C.; Thimsen, E. Plasmonic Solar Water Splitting. *Energy Environ. Sci.* **2012**, *5*, 5133−5146.
(54) Christopher, P.; Xin, H.; Linic, S. Visible-Light-Enhanced Catalytic Oxidation Reactions on Plasmonic Silver Nanostructures. *Nat. Chem.* **2011**, *3*, 467−472.
(55) Thomann, I.; Pinaud, B. A.; Chen, Z. B.; Clemens, B. M.; Jaramillo, T. F.; Brongersma, M. L. Plasmon Enhanced Solar-to-Fuel Energy Conversion. *Nano Lett.* **2011**, *11*, 3440−3446.
(56) Sigle, D. O.; Zhang, L.; Ithurria, S.; Dubertret, B.; Baumberg, J. J. Ultrathin CdSe in Plasmonic Nanogaps for Enhanced Photocatalytic Water Splitting. *J. Phys. Chem. Lett.* **2015**, *6*, 1099−1103.
(57) Naldoni, A.; Riboni, F.; Guler, U.; Boltasseva, A.; Shalaev, V. M.; Kildishev, A. V. Solar-Powered Plasmon-Enhanced Heterogeneous Catalysis. *Nanophotonics* **2016**, *5*, 112−133.
(58) Shaik, F.; Peer, I.; Jain, P. K.; Amirav, L. Plasmon-Enhanced Multicarrier Photocatalysis. *Nano Lett.* **2018**, *18*, 4370−4376.
(59) Li, J.; Cushing, S. K.; Zheng, P.; Meng, F.; Chu, D.; Wu, N. Plasmon-Induced Photonic and Energy-Transfer Enhancement of Solar Water Splitting by a Hematite Nanorod Array. *Nat. Commun.* **2013**, *4*, 2651.
(60) Thomas, K. G.; Kamat, P. V. Chromophore-Functionalized Gold Nanoparticles. *Acc. Chem. Res.* **2003**, *36*, 888−898.
(61) Catchpole, K.; Polman, A. Plasmonic Solar Cells. *Opt. Express* **2008**, *16*, 21793−21800.
(62) Jang, Y. H.; Jang, Y. G.; Kim, S.; Quan, L. N.; Chung, K.; Kim, D. H. Plasmonic Solar Cells: From Rational Design to Mechanism Overview. *Chem. Rev.* **2016**, *116*, 14982−15034.
(63) Atwater, H. A.; Polman, A. Plasmonics for Improved Photovoltaic Devices. *Nat. Mater.* **2010**, *9*, 205−213.
(64) Standridge, S. D.; Schatz, G. C.; Hupp, J. T. Distance Dependence of Plasmon-Enhanced Photocurrent in Dye-Sensitized Solar Cells. *J. Am. Chem. Soc.* **2009**, *131*, 8407−8409.
(65) Kholmicheva, N.; Moroz, P.; Rijal, U.; Bastola, E.; Uprety, P.; Liyanage, G.; Razgoniaev, A.; Ostrowski, A. D.; Zamkov, M. Plasmonic Nanocrystal Solar Cells Utilizing Strongly Confined Radiation. *ACS Nano* **2014**, *8*, 12549.
(66) Tatsuma, T.; Nishia, H.; Ishida, T. Plasmon-Induced Charge Separation: Chemistry and Wide Applications. *Chem. Sci.* **2017**, *8*, 3325−3337.
(67) Chen, X.; Zuo, L.; Fu, W.; Yan, Q.; Fan, C.; Chen, H. Insight Into the Efficiency Enhancement of Polymer Solar Cells by Incorporating Gold Nanoparticles. *Sol. Energy Mater. Sol. Cells* **2013**, *111*, 1−8.
(68) Klinkova, A.; Choueiri, R. M.; Kumacheva, E. Self-Assembled Plasmonic Nanostructures. *Chem. Soc. Rev.* **2014**, *43*, 3976−3991.
(69) Kozlovskaya, V.; Kharlampieva, E.; Khanal, B. P.; Manna, P.; Zubarev, E. R.; Tsukruk, V. V. Ultrathin Layer-by-Layer Hydrogels with Incorporated Gold Nanorods as pH-Sensitive Optical Materials. *Chem. Mater.* **2008**, *20*, 7474−7485.
(70) Govorov, A. O.; Bryant, G. W.; Zhang, W.; Skeini, T.; Lee, J.; Kotov, N. A.; Slocik, J. M.; Naik, R. R. Exciton-Plasmon Interaction and Hybrid Excitons in Semiconductor-Metal Nanoparticle Assemblies. *Nano Lett.* **2006**, *6*, 984−994.
(71) Lakowicz, J. R. *Principles of fluorescence spectroscopy*, 3rd ed.; Springer: New York, 2006.
(72) Shevchenko, E. V.; Ringler, M.; Schwemer, A.; Talapin, D. V.; Klar, T. A.; Rogach, A. L.; Feldmann, J.; Alivisatos, A. P. Self-Assembled Binary Superlattices of CdSe and Au Nanocrystals and their Fluorescence Properties. *J. Am. Chem. Soc.* **2008**, *130*, 3274−3275.
(73) Ratchford, D.; Shafiei, F.; Kim, S.; Gray, S. K.; Li, X. Manipulating Coupling Between a Single Semiconductor Quantum Dot and Single Gold Nanoparticle. *Nano Lett.* **2011**, *11*, 1049−1054.
(74) Yao, J.; Yang, M.; Duan, Y. Chemistry, Biology, and Medicine of Fluorescent Nanomaterials and Related Systems: New Insights into Biosensing, Bioimaging, Genomics, Diagnostics, and Therapy. *Chem. Rev.* **2014**, *114*, 6130−6178.
(75) Choi, Y.; Kang, T.; Lee, L. P. Plasmon resonance energy transfer (PRET)-based molecular imaging of cytochrome c in living cells. *Nano Lett.* **2009**, *9*, 85.
(76) Liu, J. M.; Chen, J. T.; Yan, X. P. Near Infrared Fluorescent Trypsin Stabilized Gold Nanoclusters as Surface Plasmon Enhanced Energy Transfer Biosensor and *in vivo* Cancer Imaging Bioprobe. *Anal. Chem.* **2013**, *85*, 3238−3245.
(77) Mangadlao, J. D.; Wang, X.; McCleese, C.; Escamilla, M.; Ramamurthy, G.; Wang, Z.; Govande, M.; Basilion, J. P.; Burda, C. Prostate-Specific Membrane Antigen Targeted Gold Nanoparticles for Theranostics of Prostate Cancer. *ACS Nano* **2018**, *12*, 3714−3725.
(78) McDonnell, J. M. Surface plasmon resonance: towards an understanding of the mechanisms of biological molecular recognition. *Curr. Opin. Chem. Biol.* **2001**, *5*, 572−577.
(79) Lausted, C.; Hu, Z.; Hood, L. Quantitative Serum Proteomics from Surface Plasmon Resonance Imaging. *Mol. Cell. Proteomics* **2008**, *7*, 2464−2474.
(80) Camposeo, A.; Persano, L.; Manco, R.; Wang, Y.; Del Carro, P.; Zhang, C.; Li, Z. Y.; Pisignano, D.; Xia, Y. Metal-Enhanced Near-Infrared Fluorescence by Micropatterned Gold Nanocages. *ACS Nano* **2015**, *9*, 10047−10054.
(81) Kim, M.; Park, K.; Jeong, E.-J.; Shin, Y.-B.; Chung, B. H. Surface Plasmon Resonance Imaging Analysis of Protein-Protein Interactions Using On-Chip-Expressed Capture Protein. *Anal. Biochem.* **2006**, *351*, 298−304.
(82) Cade, N. I.; Fruhwirth, G.; Archibald, S. J.; Ng, T.; Richards, D. A Cellular Screening Assay Using Analysis of Metal-Modified Fluorescence Lifetime. *Biophys. J.* **2010**, *98*, 2752−2757.
(83) Abadeer, N. S.; Brennan, M. R.; Wilson, W. L.; Murphy, C. J. Distance and Plasmon Wavelength Dependent Fluorescence of Molecules Bound to Silica-Coated Gold Nanorods. *ACS Nano* **2014**, *8*, 8392−8406.
(84) Lakowicz, J. R.; Ray, K.; Chowdhury, M. Plasmon-controlled fluorescence: a new paradigm in fluorescence spectroscopy. *Analyst* **2008**, *133*, 1308−1346.
(85) Lakowicz, J. R. Radiative Decay Engineering 5: Metal-Enhanced Fluorescence and Plasmon Emission. *Anal. Biochem.* **2005**, *337*, 171−194.
(86) Khatua, S.; Paulo, P. M. R.; Yuan, H.; Gupta, A.; Zijlstra, P.; Orrit, M. Resonant Plasmonic Enhancement of Single-Molecule Fluorescence by Individual Gold Nanorods. *ACS Nano* **2014**, *8*, 4440−4449.
(87) Sen, T.; Patra, A. Recent Advances in Energy Transfer Processes in Gold-Nanoparticle-Based Assemblies. *J. Phys. Chem. C* **2012**, *116*, 17307−17317.
(88) Heydari, E.; Pastoriza-Santos, I.; Flehr, R.; Liz-Marzán, L. M.; Stumpe, J. Nanoplasmonic Enhancement of the Emission of Semiconductor Polymer Composites. *J. Phys. Chem. C* **2013**, *117*, 16577−16583.
(89) Demchenko, A. P. Nanoparticles and Nanocomposites for Fluorescence Sensing And Imaging. *Methods Appl. Fluoresc.* **2013**, *1*, 022001.
(90) Malicka, J.; Gryczynski, I.; Gryczynski, Z.; Lakowicz, J. R. Effects of Fluorophore-To-Silver Distance on the Emission of

DOI: 10.1021/jacs.9b04697
J. Am. Chem. Soc. 2019, 141, 11286−11297

Cyanine−Dye-Labeled Oligonucleotides. *Anal. Biochem.* **2003**, *315*, 57−66.
(91) Tovmachenko, O. G.; Graf, C.; van den Heuvel, D. J.; van Blaaderen, A.; Gerritsen, H. C. Fluorescence Enhancement by Metal-Core/Silica-Shell Nanoparticles. *Adv. Mater.* **2006**, *18*, 91−95.
(92) Lee, S. Y.; Nakaya, K.; Hayashi, T.; Hara, M. Quantitative Study of the Gold-Enhanced Fluorescence of CdSe/ZnS Nanocrystals as a Function of Distance Using an AFM Probe. *Phys. Chem. Chem. Phys.* **2009**, *11*, 4403−4409.
(93) Förster, T. Zwischenmolekulare Energiewanderung und Fluoreszenz. *Ann. Phys.* **1948**, *437*, 55.
(94) Zhang, X.; Marocico, C. A.; Lunz, M.; Gerard, V. A.; Gun'ko, Y. K.; Lesnyak, V.; Gaponik, N.; Susha, A. S.; Rogach, A. L.; Bradley, A. L. Wavelength, Concentration, and Distance Dependence of Nonradiative Energy Transfer to a Plane of Gold Nanoparticles. *ACS Nano* **2012**, *6*, 9283−9290.
(95) Gersten, J. I.; Nitzan, A. Spectroscopic Properties of Molecules Interacting With Small Dielectric Particles. *J. Chem. Phys.* **1981**, *75*, 1139.
(96) Moroz, A. Non-Radiative Decay of a Dipole Emitter Close to a Metallic Nanoparticle: Importance of Higher-Order Multipole Contributions. *Opt. Commun.* **2010**, *283*, 2277−2287.
(97) Marocico, C. A.; Zhang, X.; Bradley, A. L. A Theoretical Investigation of the Influence of Gold Nanosphere Size on the Decay and Energy Transfer Rates and Efficiencies of Quantum Emitters. *J. Chem. Phys.* **2016**, *144*, 024108.
(98) Fu, Y.; Zhang, J.; Lakowicz, J. R. Plasmon-Enhanced Fluorescence from Single Fluorophores End-Linked to Gold Nanorods. *J. Am. Chem. Soc.* **2010**, *132*, 5540−5541.
(99) Gandra, N.; Portz, C.; Tian, L.; Tang, R.; Xu, B.; Achilefu, S.; Singamaneni, S. Probing Distance-Dependent Plasmon-Enhanced Near-Infrared Fluorescence Using Polyelectrolyte Multilayers as Dielectric Spacers. *Angew. Chem., Int. Ed.* **2014**, *53*, 866.
(100) Li, J.; Li, C.; Aroca, R. F. Plasmon-Enhanced Fluorescence Spectroscopy. *Chem. Soc. Rev.* **2017**, *46*, 3962.
(101) Acuna, G. P.; Möller, F. M.; Holzmeister, P.; Beater, S.; Lalkens, B.; Tinnefeld, P. Fluorescence Enhancement at Docking Sites of DNA-Directed Self-Assembled Nanoantennas. *Science* **2012**, *338*, 506−510.
(102) Puchkova, A.; Vietz, C.; Pibiri, E.; Wünsch, B.; Sanz Paz, M.; Acuna, G. P.; Tinnefeld, P. DNA Origami Nanoantennas with over 5000-Fold Fluorescence Enhancement and Single-Molecule Detection at 25 um. *Nano Lett.* **2015**, *15*, 8354−8359.
(103) Li, J.; Krasavin, A. V.; Webster, L.; Segovia, P.; Zayats, A. V.; Richards, D. Spectral Variation of Fluorescence Lifetime Near Single Metal Nanoparticles. *Sci. Rep.* **2016**, *6*, 21349.
(104) Bardhan, R.; Grady, N. K.; Cole, J. R.; Joshi, A.; Halas, N. J. Fluorescence Enhancement by Au Nanostructures: Nanoshells and Nanorods. *ACS Nano* **2009**, *3*, 744−752.
(105) Park, S.; Pelton, M.; Liu, M.; Guyot-Sionnest, P.; Scherer, N. F. Ultrafast Resonant Dynamics of Surface Plasmons in Gold Nanorods. *J. Phys. Chem. C* **2007**, *111*, 116.
(106) Sönnichsen, C.; Franzl, T.; Wilk, T.; von Plessen, G.; Feldmann, J.; Wilson, O.; Mulvaney, P. Drastic Reduction of Plasmon Damping in Gold Nanorods. *Phys. Rev. Lett.* **2002**, *88*, 077402.
(107) Zhao, T.; Jarrett, J. W.; Johnson, J. S.; Park, K.; Vaia, R. A.; Knappenberger, K. L. Plasmon Dephasing in Gold Nanorods Studied Using Single-Nanoparticle Interferometric Nonlinear Optical Microscopy. *J. Phys. Chem. C* **2016**, *120*, 4071.
(108) Vigderman, L.; Khanal, B. P.; Zubarev, E. R. Functional gold nanorods: synthesis, self-assembly, and sensing applications. *Adv. Mater.* **2012**, *24*, 4811−4841.
(109) Singh, M. P.; Strouse, G. F. Involvement of the LSPR spectral overlap for energy transfer between a dye and Au nanoparticle. *J. Am. Chem. Soc.* **2010**, *132*, 9383.
(110) Samanta, A.; Zhou, Y.; Zou, S.; Yan, H.; Liu, Y. Fluorescence Quenching of Quantum Dots by Gold Nanoparticles: A Potential Long Range Spectroscopic Ruler. *Nano Lett.* **2014**, *14*, 5052.
(111) Wang, W.; Kapur, A.; Ji, X.; Safi, M.; Palui, G.; Palomo, V.; Dawson, P. E.; Mattoussi, H. Photoligation of an Amphiphilic Polymer with Mixed Coordination Provides Compact and Reactive Quantum Dots. *J. Am. Chem. Soc.* **2015**, *137*, 5438−5451.
(112) Kamat, P. V.; Barazzouk, S.; Hotchandani, S. Electrochemical Modulation of Fluorophore Emission on a Nanostructured Gold Film. *Angew. Chem., Int. Ed.* **2002**, *41*, 2764−7.
(113) Ahmadi, T. S.; Logunov, S. L.; El-Sayed, M. A. *J. Phys. Chem.* **1996**, *100*, 8053−8056.
(114) Logunov, S. L.; Ahmadi, T. S.; El-Sayed, M. A. *J. Phys. Chem. B* **1997**, *101*, 3713−3719.
(115) Khon, E.; Mereshchenko, A.; Tarnovsky, A. N.; Acharya, K.; Klinkova, A.; Hewa-Kasakarage, N. N.; Nemitz, I.; Zamkov, M. Suppression of the plasmon resonance in Au/CdS colloidal nanocomposites. *Nano Lett.* **2011**, *11*, 1792−1799.
(116) Moroz, P.; Razgoniaeva, N.; He, Y.; Jensen, G.; Eckard, H.; Lu, H. P.; Zamkov, M. Tracking the Energy Flow on Nanoscale *via* Sample-Transmitted Excitation Photoluminescence Spectroscopy. *ACS Nano* **2017**, *11*, 4191−4197.
(117) Moroz, P.; Razgoniaeva, N.; Vore, A.; Eckard, H.; Kholmicheva, N.; McDarby, A.; Razgoniaev, A. O.; Ostrowski, A. D.; Khon, D.; Zamkov, M. Plasmon-Induced Energy Transfer: When the Game is Worth the Candle. *ACS Photonics* **2017**, *4*, 2290−2297.
(118) Moroz, P.; Klein, W. P.; Akers, K.; Vore, A.; Kholmicheva, N.; Razgoniaeva, N.; Khon, D.; Díaz, S. A.; Medintz, I. L.; Zamkov, M. Lifting the Spectral Crosstalk in Multifluorophore Assemblies. *J. Phys. Chem. C* **2017**, *121*, 26226−26232.
(119) Moroz, P.; Jin, Z.; Sugiyama, Y.; Lara, D.; Razgoniaeva, N.; Yang, M.; Kholmicheva, N.; Khon, D.; Mattoussi, H.; Zamkov, M. The Competition of Charge and Energy Transfer Processes in Donor-Acceptor Fluorescence Pairs: Calibrating the Spectroscopic Ruler. *ACS Nano* **2018**, *12*, 5657−5665.
(120) Mujumdar, R. B.; Ernst, L. A.; Mujumdar, S. R.; Lewis, C. J.; Waggoner, A. S. Cyanine dye labeling reagents: Sulfoindocyanine succinimidyl esters. *Bioconjugate Chem.* **1993**, *4*, 105−111.
(121) Massey, M.; Kim, H.; Conroy, E. M.; Algar, W. R. Expanded Quantum Dot-Based Concentric Förster Resonance Energy Transfer: Adding and Characterizing Energy-Transfer Pathways for Triply Multiplexed Biosensing. *J. Phys. Chem. C* **2017**, *121*, 13345−13356.
(122) Grigoriev, V.; Bonod, N.; Wenger, J.; Stout, B. Optimizing Nanoparticle Designs for Ideal Absorption of Light. *ACS Photonics* **2015**, *2*, 263−270.
(123) Song, J.-H.; Atay, T.; Shi, S.; Urabe, H.; Nurmikko, A. V. Large Enhancement of Fluorescence Efficiency from CdSe/ZnS Quantum Dots Induced by Resonant Coupling to Spatially Controlled Surface Plasmons. *Nano Lett.* **2005**, *5*, 1557−1561.
(124) Fort, E.; Gresillon, S. Surface enhanced fluorescence. *J. Phys. D: Appl. Phys.* **2008**, *41*, 013001.
(125) Pellegrotti, J. V.; Acuna, G. P.; Puchkova, A.; Holzmeister, P.; Gietl, A.; Lalkens, B.; Stefani, F. D.; Tinnefeld, P. Controlled Reduction of Photobleaching in DNA Origami-Gold Nanoparticle Hybrids. *Nano Lett.* **2014**, *14*, 2831−2836.
(126) Mondal, N.; Samanta, A. Ultrafast Charge Transfer and Trapping Dynamics in a Colloidal Mixture of Similarly Charged CdTe Quantum Dots and Silver Nanoparticles. *J. Phys. Chem. C* **2016**, *120*, 650−658.
(127) Murphy, G. P.; Gough, J. J.; Higgins, L. J.; Karanikolas, V. D.; Wilson, K. M.; Garcia Coindreau, J. A.; Zubialevich, V. Z.; Parbrook, P. J.; Bradley, A. L. Ag colloids and arrays for plasmonic nonradiative energy transfer from quantum dots to a quantum well. *Nanotechnology* **2017**, *28*, 115401.
(128) Wax, T. J.; Dey, S.; Chen, S.; Luo, Y.; Zou, S.; Zhao, J. Excitation Wavelength-Dependent Photoluminescence Decay of Hybrid Gold/Quantum Dot Nanostructures. *ACS Omega* **2018**, *3*, 14151−14156.
(129) Aldeek, F.; Safi, M.; Zhan, N.; Palui, G.; Mattoussi, H. Understanding the Self-Assembly of Proteins onto Gold Nanoparticles and Quantum Dots Driven by Metal-Histidine Coordination. *ACS Nano* **2013**, *7*, 10197−10210.

DOI: 10.1021/jacs.9b04697
J. Am. Chem. Soc. 2019, 141, 11286−11297

(130) Pons, T.; Medintz, I. L.; Sapsford, K. E.; Higashiya, S.; Grimes, A. F.; English, D. S.; Mattoussi, H. On the quenching of semiconductor quantum dot photoluminescence by proximal gold nanoparticles. *Nano Lett.* **2007**, *7*, 3157−3164.
(131) Oh, E.; Huston, A. L.; Shabaev, A.; Efros, A.; Currie, M.; Susumu, K.; Bussmann, K.; Goswami, R.; Fatemi, F. K.; Medintz, I. L. Energy Transfer Sensitization of Luminescent Gold Nanoclusters: More than Just the Classical Förster Mechanism. *Sci. Rep.* **2016**, *6*, 35538.

DOI: 10.1021/jacs.9b04697
J. Am. Chem. Soc. 2019, 141, 11286−11297